Planar Array Capacitive Imaging Sensor Design Optimisation

Carl Tholin-Chittenden, Manucher Soleimani

***Abstract*—Electrical Capacitance Tomography (ECT) is used in many industries as a non-invasive detection and measurement method which works by finding permittivity changes in a viewing region. This usually consists of sensor electrodes surrounding a region of interest however this is not always possible as sometimes the viewing region is only accessible from a single side. In this case a planar array ECT system can be used where the electrodes are all laid out on a co-planar surface. Initial simulation results indicated some features of sensor design which might aid image reconstructions. 5 new electrode configurations were designed which incorporated these features in different ways. The designs were tested on their ability to reproduce a wooden block suspended in air and a water bottle buried in sand. Their performance was judged based on distance/depth detection of the block/water bottle and the shape of the reconstruction. Singular Value Decomposition (SVD) analysis was also performed on each sensor design to show their theoretical ability to reproduce the permittivity of the viewing region. Previously similar work managed to reliably reconstruct objects at distances of 60mm from the sensor. But in this paper, with a smaller sensor head, up to 90mm was achieved with good accuracy. Combining the sensor designs together into a single sensor created the Combined Sensor which was able to reconstruct objects with a much greater reliability and was less susceptible to error or noise. With the right set up the Combined Sensor was able to achieve up to 120mm of depth detection. Also the combined sensor was able to detect a buried water bottle in sand up to 50mm. Further simulation results on the Combined Sensor indicated that using up to 100 unique sensor configurations in the combined sensor was beneficial but after 100 the amount of additional information gained was not significant. The results showed that the sensor head design can be optimised in order to produce improved reconstruction for planar array ECT. This improvement means that planar array ECT could potentially become a viable option for applications such as landmine detection, particularly finding non-metallic objects which can not be picked up with conventional landmine detection techniques such as metal detectors.**

***Index Terms*—Electrical Capacitance Tomography, Planar Array, Sensor Optimisation**

I. Introduction

Current landmine detection techniques struggle to find and identify modern landmines fabricated from sophisticated non-metallic materials incorporated with advanced electronics [1]. This increase in sophistication from the manufacturers of landmines needs to be met with new technologies able to effectively detect these landmines and aid in their clearance.

One method which has potential to be used as a landmine detection technique is Electrical Capacitance Tomography (ECT) [2]. ECT is a method of non-invasive imaging by using electrodes that measure capacitance, around a viewing region, to build up a permittivity distribution. Most commonly the electrodes surround the viewing region on all sides which creates the best possible reconstruction as the capacitance is measured across the area of interest [3]. However in some applications this is not possible as all of the sides may not be accessible such as in landmine detection in which only 1 side is available. In this case the conventional parallel-plate capacitor has been replaced with a fringing-field capacitor [4] which opens up the area that will affect the capacitance between the plates and allows the electrodes to be arranged on a co-planar surface.

Planar array ECT is an attractive prospect for landmine detection as it has the potential to find landmines made out of any material, not just metallic landmines, as well as theoretically being able to distinguish between different materials inside the same landmine which would therefore allow for greater accuracies in classification. Another benefit includes the fact that it can produce 3-dimensional images of the viewing area which other landmine detection techniques don't do.

In order to use planar array ECT for landmine detection the technology needs to be further developed as in it's current state it is not accurate enough for the level required for a feasible landmine detection technique. Some early research has focused on using planar 10μm to 1mm wide electrodes in detecting flowing particles [5]. This produced good results and showed the technology had potential but as it was on such a small scale it didn't show if the technology could be scaled up. Anti-personnel landmines tend to be buried only a few centimetres from the surface [6] but this would require larger electrodes. Research into electrode shape for a planar array system revealed that the maximum detectable depth was approximately equal to the spacing between the electrodes [7] as this therefore means that, for it to be used in landmine detection, the smallest possible sensor head is 2cm. Any sensor head designed therefore needs to be far bigger if then entire body of the landmine is to be detected too. The most relevant research using a planar array ECT sensor showed that with a 17cm $\times$ 17cm sensor a wooden block suspended above in air could be detected 6cm away [8]. This sensor head consisted of 12 rectangular electrodes arranged in a 3×4 grid and is a good starting point for a design capable of detecting landmines.

To detect landmines a sensor would firstly need to be able to reconstruct an object buried as deep as possible relative to the sensor head design. Simply increasing the distance between the sensor electrodes would increase the depth detection but it

Engineering Tomography Lab (ETL), University of Bath, Department of Electronics & Electrical Engineering, Bath BA2 7AY, United Kingdom (C.Tholin-Chittenden@bath.ac.uk, M.Soleimani@bath.ac.uk)

would decreases the sensitivity of the measurement, thus increasing reconstruction error from noise, as well as decreasing reconstruction resolution. Therefore if the depth detection can be increased without moving the electrodes further apart then the objects can be more accurately reconstructed.

This paper aims to build upon the planar array ECT sensor head design used by Ye et al. (2013) [8] and identify features of ECT sensor designs which allow object depth reconstruction to be improved without increasing the size of the sensor head. By firstly simulating many unique sensors and analysing their theoretical performance, design features can be identified which could improve sensor performance. These features will be used in new sensor designs to be constructed and then tested to see how well their depth and location detection of an object is.

II. Electrical Capacitance Tomography

ECT is the method of constructing a permittivity distribution based on a number of capacitance measurements by taking capacitance measurements between many electrodes in an array. The calculation of the permittivity distribution from the capacitance measurements is performed in 2 stages. Firstly there is the "forward problem" followed by image reconstruction, often referred to as the "inverse problem".

The forward problem is where the physical and electromagnetic properties of the device and viewing region are modelled in order to produce results on the relationship between the capacitances measured and how they relate to the permittivity of the viewing region. Using Gauss's electricity law we can derive Poisson's equation and as the net electric flux across all of the electrode surfaces is zero we can say:

$$\nabla \cdot (-\varepsilon \nabla \phi) = 0 \tag{1}$$

where ε is the permittivity distribution, ϕ is the electric potential distribution and $\nabla\cdot$ is the divergence operator. Using this Partial Differential Equation (PDE) we can calculate the electric potential for a given permittivity distribution in our 3D environment (x, y, z). To get the charge on the sensing electrode the surface integral of the electric flux density can be taken for the electrode area Ω:

$$C = \frac{1}{V} \oint_{\Omega} \varepsilon \mathbf{E} \cdot \hat{n} d\omega \tag{2}$$

where C is the inter electrode capacitance, V is the electric potential on the excitation electrode, $\hat{n}$ is a vector to the normal of the electrode surface and $\mathbf{E}$ is the electric field distribution. It can be seen that capacitance is a function of the permittivity and this forms the start of the image reconstruction.

$$\Delta C = J \Delta \varepsilon \tag{3}$$

where J is the Jacobian. By using a Jacobian a permittivity distribution, $\Delta\varepsilon$ can be found from a set of capacitance measurements, ΔC, by solving this as an inverse problem. The reconstruction is not well-posed as there is not a single valid solution and small changes in input means big changes in the output. Also the physics of electric fields and permittivity mean that the problem is also ill-conditioned. The inverse problem attempts to solve equation 3 for permittivity but as the number of voxels, N, is much larger than number of measurements, M, J will not be square so it cannot be inverted. Therefore it must be solved alternatively. One method is the least squares solution or alternatively by using the Moore-Penrose generalised inverse [9]. But due to the ill-posedness of the initial problem some form of regularisation is required. Tikhonov Regularisation [10] and Landweber Iteration [11] are 2 examples of solving inverse problems with regularisation. Tikhonov regularisation is a form of least-squares solver which attempts to fit the data to a solution shown by the following:

$$\Delta \varepsilon = \left(J^T J + \alpha^2 \Gamma \right)^{-1} J^T \Delta C \tag{4}$$

where α^2 is the scaling of the regularisation matrix, Γ, which is the identity. This value is used to affect how much the added term controls the final solution.

SVD Analysis: A useful comparison method of the Jacobian is Singular Value Decomposition (SVD). SVD is a method splitting up a dataset in order to generalise some of it's properties. This is done by separating the dataset J into the following sets [12]:

$$J = U \Sigma V^T \tag{5}$$

where U is made up of the eigenvectors of JJ^T and V is made up of the eigenvectors of $J^T J$. Σ is a diagonal matrix containing the singular values of J. The singular values are ordered such that $\Sigma = diag\left[\sigma_1 \geq \sigma_2 \geq \cdots \geq \sigma_N\right]$.

What the singular values of Σ are representing is essentially how much of an effect that particular column vector of J has on the final solution. For the smaller singular values, the solution is going to be less affected by the data. This means that for noise and errors in the input, these column vectors with small singular values are going to amplify this noise/error much more and thus affect the final solution to a greater extent. If the singular values can be kept as big as possible, then there is going to be more useful data in the solution which makes the solution more accurate. SVD can be used to theoretically evaluate the ability of a Jacobian to reconstruct data effectively [13].

III. DeTECT (Demining Technology ECT) Software

As a part of this investigation a software toolbox was developed called DeTECT . It is capable of taking CAD schematics of the sensor head to set up the simulation environment, solves

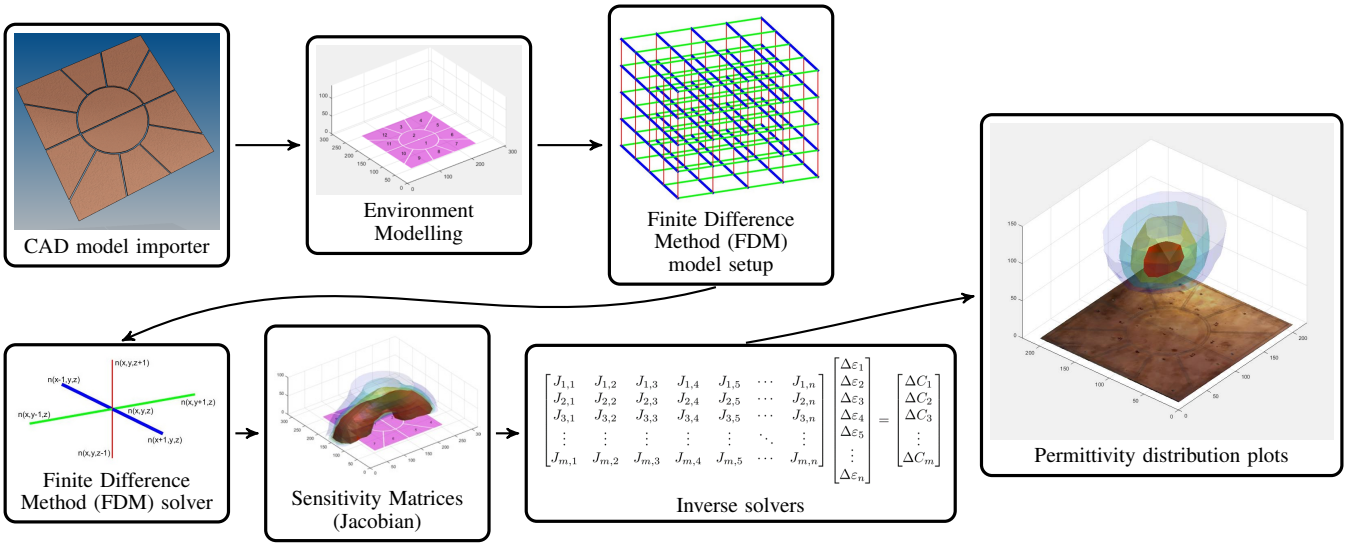

Fig. 1: Flowchart of DeTECT software toolbox.

this model and then calculates a permittivity distribution based on input capacitance readings. Figure 1 shows a flowchart of the process that DeTECT uses.

The simulation method used is the Finite Difference Method (FDM). DeTECT is able to use FDM as the viewing region is rectangular and therefore fits nicely with the grid shape of FDM. During early development of DeTECT , the results from the FDM model were compared with a Finite Element Method (FEM) model and the results were shown to be consistent with each other. Therefore FDM was selected for it's other benefits of simplicity and ease of manipulation without compromising accuracy. Using FDM also then allows a comparison and verification to be made with existing ECT software such as those using FEM [8].

The CAD importer allows complex shapes to be drawn and immediately imported to the software easily. DeTECT can then change various parameters of the viewing region such as height, width, length, sensor location, sensor orientation and more.

The FDM model calculates values at each node, n in the grid of N nodes where $N = X \times Y \times Z$ and X, Y and Y are the number of nodes in the x, y and z directions respectively. Node n can be found by:

$$n = XY(z-1) + X(y-1) + x \tag{6}$$

The PDE, equation 1, can be derived into a FDM equation to describe the relationship between a node and its neighbours. From equation 1 we get:

$$\begin{aligned}
\nabla \cdot (-\varepsilon \nabla \phi) = &-\varepsilon(\phi_{x+1,y,z} + \phi_{x-1,y,z} - 2\phi_{x,y,z}) \\
&-\varepsilon(\phi_{x,y+1,z} + \phi_{x,y-1,z} - 2\phi_{x,y,z}) \\
&-\varepsilon(\phi_{x,y,z+1} + \phi_{x,y,z-1} - 2\phi_{x,y,z}) \\
0 = &-\varepsilon(\phi_{x+1,y,z} + \phi_{x-1,y,z} \\
&+ \phi_{x,y+1,z} + \phi_{x,y-1,z} \\
&+ \phi_{x,y,z+1} + \phi_{x,y,z-1} \\
&- 6\phi_{x,y,z})
\end{aligned} \tag{7}$$

Where ε is a vector made up of the permittivity of each individual node. The electric potential at a node is essentially the sum of permittivities and electric potential of adjacent nodes (not diagonal nodes) divided by the sum of permittivities of the adjacent nodes:

$$\phi_{x,y,z} = \frac{\sum_i \sum_j \sum_k \varepsilon_{x+i,y+j,z+k} \phi_{x+i,y+j,z+k}}{\sum_i \sum_j \sum_k \varepsilon_{x+i,y+j,z+k}} \tag{8}$$

where $i, j, k \in \{-1, 1\}$ to get each of the adjacent nodes. The excitation electrode has an electric potential of V on it and so therefore any nodes that make up part of this electrode are given an initial boundary electric potential value of V. The electric potentials are weighted based on their values of permittivity but this is often negligible as the initial permittivity distributions used are uniform. The DeTECT software calculates this using a linear solver.

The final step of the forward problem is creating the Jacobian which will be used to translate between capacitance and dielectric permittivity of the viewing region. To calculate each Jacobian value the electric field distributions are calculated for each electrode combination, m, of the selected pair, $m1$ and $m2$. These are then used in the equation [14]:

$$J_m^n = \frac{E_{m1}^n \cdot E_{m2}^n}{V_{m1} V_{m2}} \tag{9}$$

This is repeated for each electrode combination and so the rows of this Jacobian essentially become a sensitivity map for that particular combination.

One issue encountered with the DeTECT software lies in how the forward model is set up based on the electrode layout design. As the software converts a detailed CAD model into a discrete nodal FDM model some of the detail is lost. High resolution levels are usually required in order to fully represent that data (20+ voxels per dimension).

IV. Simulation Results

The environment modelling of the DeTECT software can be used to simulate the sensor design which will result in theoretical capacitance measurements and the Jacobian for that particular sensor design. This can therefore be utilised to compare designs before physically manufacturing them.

The first problem is to create sensor designs to be simulated. The most important aspects of the sensor design for sensor performance are the electrode shapes, layouts and spacings [7]. Some work has already been done on electrode shape and its affect on depth, location and material characterisation detection. However as there is no clear formula for planar array capacitive imaging sensor design a novel method of design can be implemented. Also this work on design does not include looking at the effect of different shapes in combination as part of a multiple electrode sensor.

To get new electrode shapes and layouts a procedural generation method will be used to come up with designs. This will both generate new electrode shapes, as well as laying them out in unique configurations. The generation will always attempt to keep the size of each electrode as consistent to the other electrodes as possible.

The procedural generation has 4 different design modes. The first is a random generation, the second is a 1 line of symmetry random generation and the third is a 2 line of symmetry random generation. The fourth design mode splits the sensor area into quadrants but then randomly populates each quadrant with electrodes as with design mode 1.

Design mode 1 works by firstly randomly filling an area (the overall sensor boundary) with a chosen number of electrodes. The electrodes are randomly populated and the only constraint is that the electrodes are joined up and no electrode is split in multiple locations on the sensor head. An example of the design mode can be seen in figure 2.

Design mode 2 uses a line of symmetry combined with the random electrode shape and layout. This removes an element of randomness in the choice of the electrode layouts and shapes and there is reason to believe that symmetry will be beneficial in this application due to the physics of how capacitance works. Half of the sensor design area is randomly generated as with design mode 1 and then this is mirrored to the other area.

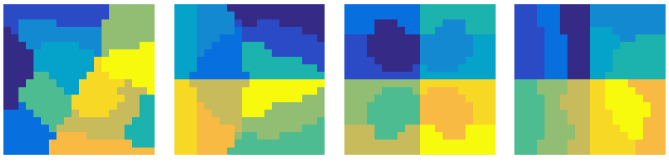

Fig. 2: Examples of each design modes resulting sensor design (each electrode is coloured uniquely).

Design mode 3 is the same as design mode 2 but instead 2 lines of symmetry are used. The random electrode generation is only performed for a quadrant of the overall sensor area for a quarter of the desired electrodes. This in then mirrored for each quadrant resulting in 4 areas of electrodes with 2 lines of symmetry.

Finally design mode 4 has 4 quadrants as with design mode 3 but no symmetry. Each quadrant is randomly generated and this will be used to compare the effectiveness of the straight lines and layouts with quadrants but without the element of symmetry. Direct comparison between design modes 3 and 4 will be possible for this reason.

Over 7000 unique sensor designs were procedurally generated with the design modes 1-4. Each sensor design was then simulated with DeTECT and the Jacobian for each was found. SVD analysis was then performed on each Jacobian to see how many singular values each had with a value greater than a noise threshold of 1%. This is a reasonable noise threshold to use and should allow a comparison to be made.

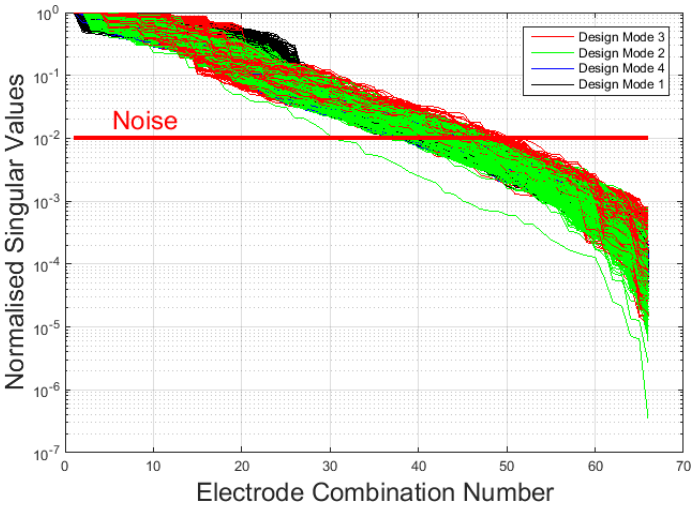

Fig. 3: SVD analysis of procedurally generated sensor designs.

Figure 3 shows how each design mode compares to each other in a theoretical ability to reconstruct images. The more electrode combinations which have a singular value above the noise threshold, the better the sensor design should be at reconstructing images. The sensor designs which achieve

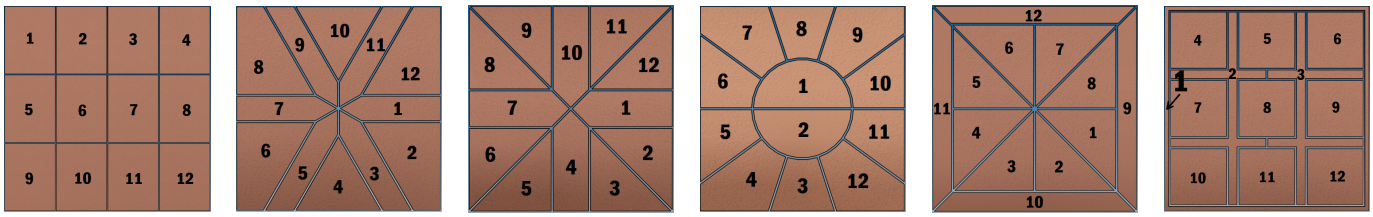

Fig. 4: Sensor designs with electrode indices.

the most singular values above 1% noise is by far those procedurally generated with design mode 3 where the best sensor design has 50 singular values above the noise threshold. Of the top 100 sensors 77 were made with design mode 3, 23 were made with design mode 2 none were made with design mode 1 or 4. The best design mode 1 sensor ranked 142nd and the best design mode 4 sensor ranked 326th.

This indicates 2 things. Firstly it is clear that combining the sensors into distinct areas does not in itself seem to be beneficial. Design mode 3 and 4 both have 4 distinct quadrants of electrodes and perform best and worst respectively. This lends nicely to the second conclusion that symmetry is very powerful. Design mode 1 and 4 have no symmetry and perform very poorly. Design mode 2 has some symmetry and performs better. But design mode 3 has 2 lines of symmetry and performs far better than the other design modes in creating sensor designs. It could be other factors which are making design mode 3 perform better but it makes sense that symmetry would have some bearing on performance as it means that electrodes have more of their perimeters touching another same size electrode and electric fields created will be more uniform.

V. Sensor Design Optimisation

Sensor Design & Construction

To test conclusions made from the simulation results in an experimental manner, 5 new planar array ECT sensor heads were designed shown in figure 4. These designs were not aimed at finding one which is fully optimised but instead working out which features of the sensor performs better. Sensor 1 attempts to maximise lines of symmetry as the simulation results showed that more lines could lead to an improvement in performance. Sensor 2 also attempts to maximise the lines of the symmetry in the design but with a more uniform electrode size and shape distribution. Sensor 3 adds a curved edge to the otherwise very straight lined designs but still maintaining symmetry. A lot of the best simulation designs had an element of curvature surrounded by straight lines. Sensor 4 inverts Sensor 3 by putting a level of long electrodes around the outside surrounding a group of triangular electrodes in the middle. A lot of the best designs from the simulation results contained narrow electrodes surrounding rounder electrodes. Sensor 5 uses this concept with the basic grid shape of the Original Sensor. The design of Sensor 5 should also theoretically increase the capacitance readings as the shortest distance between sensors has been reduced due to the inter-electrode electrodes.

Five sensor designs should be enough to give a good analysis of sensor design. They are all very different and each aims to investigate a particular feature identified by the simulation results and theory on sensor design.

All sensor designs were constructed in an identical way. An overall sensor dimension of 200mm x 200mm square for each electrode array was used. All the electrodes used a minimum gap width of 1mm between each other in order to give the electrodes spacing as well as keep the amount of usable surface area as even as possible between designs. Each sensor has 12 electrodes which leads to M as 66 unique combinations of electrodes. The material used for each sensor was a copper plated PCB board which has copper on both sides. The electrode layout design was cut out on the front whilst keeping the back as a single piece of copper across the board. The back plate was then grounded which will absorb back-capacitance and prevent the electrodes from being affected by changes in permittivity behind.

As well as the new designs, the Original Sensor Design used previously by Ye et al. (2013) [8], was reconstructed to match the fixed design constraints of the other sensors. This was to allow for comparison of the new design with an existing design. All the sensors are identical in construction apart from the electrode shape and layout. However due to the varying shape of the electrodes, the electrical connection to the electrodes by the signal cables could not be kept constant and for this reason there is some slight variation in these electrical connections between the sensor designs. This should have a negligible effect on the resulting measurements as the surface area of these small connections are very small compared with the overall electrode surface area so any stray capacitance shouldn't have a big effect.

As capacitance is proportional to surface area the capacitance magnitude is always affected by the smallest surface area electrode so the surface areas of the electrodes were designed as evenly as possible across all 12 electrodes. All sensor designs have an average electrode surface area around 3000 mm^2 where the biggest individual electrode surface area variation is 37% of the average. However the overall average variation of surface area is only 11.5% which is a good value to show

that the surface areas have been kept as consistent as possible. Some of the designs however did not allow surface areas to be even such as sensor 1. Sensors 2, 4 and 5 all have identical surface areas across each electrode, but sensor 1 and 3 do not so this will allow for a comparison on surface areas and it's affect on reconstruction.

The performance of the sensor designs will be assessed based on the optimisation criteria.

Optimisation Criteria

SVD analysis: This is the number of singular values obtained from SVD which lie above a chosen noise threshold. This will give a theoretical view on which sensor head design is best.

Depth Detection: The difference between reconstructed and actual distances of the object edge to the sensor will be compared for each sensor design. Minimising difference will be better as this shows improved accuracy.

Location Detection: The reconstructed object centre will be compared to the actual location of the object centre. Minimising the error will show a better sensor design.

VI. Experimental Results

Individual Sensors

In order to validate the sensor construction theoretical capacitance values taken from `DeTECT` were compared to actual measured capacitances from the sensors. `DeTECT` calculates theoretical values at a different scale to the real measured values but comparisons can still be made if both sets of measurements are normalised.

Fig. 5: PTL 300E device for capturing capacitance data and experimental setup.

The PTL 300E, figure 5, was the device used to capture the capacitance data. The 12 electrodes of the sensor head are plugged in to the 12 connections on the front of the device and then capacitance data can be captured live to a connected PC at up to 300 frames per second.

Figure 6 shows a comparison of measured and simulated capacitance for two of the sensor designs. The values have been normalised in order to allow for a visual comparison. The simulation will not produce accurate capacitance magnitudes due to the way the modelling is performed and the PTL device could be amplifying the measured capacitance values so it is not known what the collected measurements refer to. This is because the device is designed to be used with industry standard sensors attached. It can be quite clearly seen that the pattern of the measurements between the simulated and measured capacitance values is very similar. This indicates that the simulation is working correctly and also that the sensor heads were manufactured correctly and are operating in practice as expected.

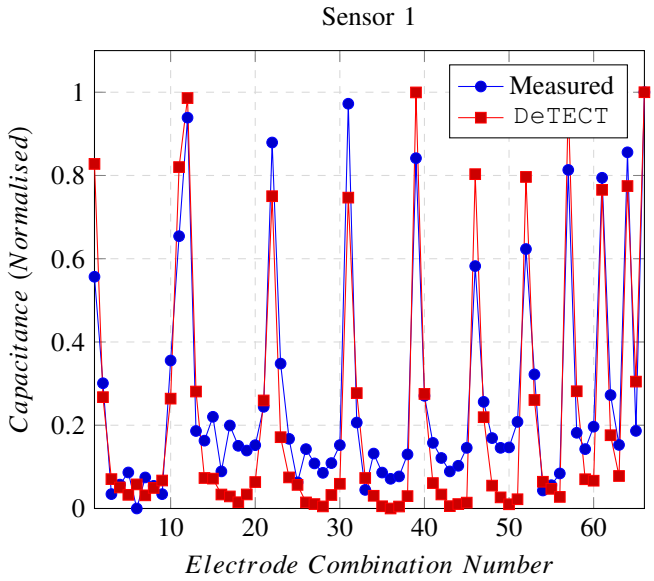

Fig. 6: Comparison between measured and simulated capacitance values of Sensor 3.

The `DeTECT` software also calculates electric field distributions for the sensor designs and from this sensitivity plots can be produced to show what regions of permittivity change the sensor designs are most sensitive to.

The surfaces on the sensitivity plots in figure 7 show how sensitive that region is to the final reconstruction. An isosurface of the sensitivity plots has been found to show the shape of the reach of the sensors but the isosurface value is different for each of them shown by the number by the plot. The value of this number indicates how much a change in this area will affect the sensors measurement readings with a bigger number indicating a bigger change in capacitance measurements. The shapes found show the direction and area that the sensors are most sensitive to. All of the sensors, except sensor 4, have a very wide base shape and then point upwards. This indicates that they will be good at detecting object locations close to the sensor but will struggle when the object is further away. Sensor 4 however has a much more directed upward shape and isn't so wide at the bottom. This indicates that it will be able to detect object better at distance as well as locate them more accurately. Sensor 4 has outer electrodes which encase the central electrodes and it could be seen that this feature is making the sensitivity region of the sensor much more directed which could be desirable. The value of the isosurface gives some indication on the magnitude

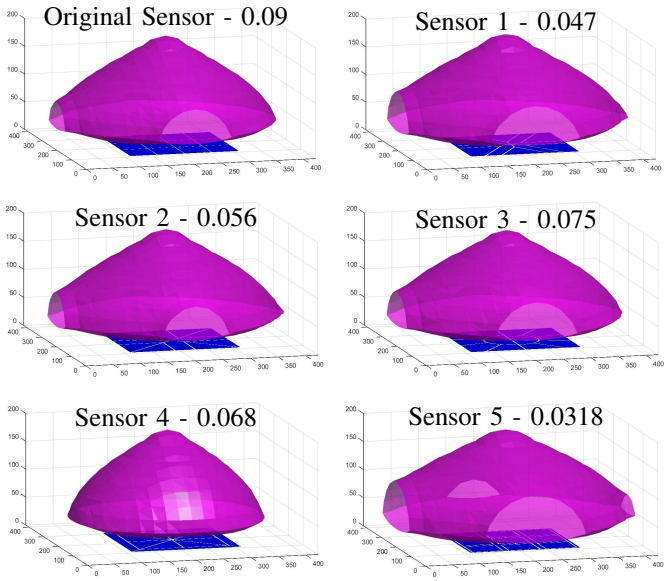

Fig. 7: A single isosurface of the sensitivity plots of each sensor design and the isosurface value.

of the final reconstructions. It would make sense that the sensitivity plots with a larger isosurface value at the same distance will reconstruct higher permittivities and therefore are more likely to reconstruct objects which cause smaller changes in capacitance. This could mean they will perform better at detecting bigger distances. Sensor 5 has by far the smallest isosurface value at 0.0318 and the original sensor has the highest at 0.9.

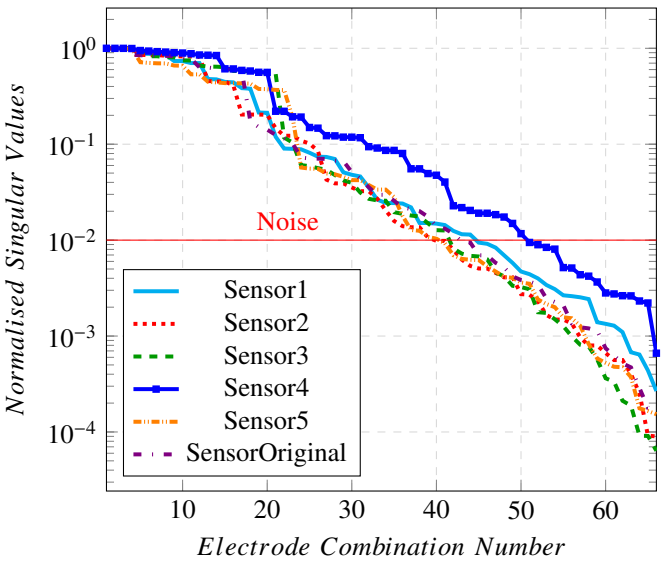

Fig. 8: SVD analysis of all sensor designs at a resolution of 30 voxels per dimension.

SVD analysis: The sensors can be compared on their ability to construct an image by SVD analysis on their Jacobians [12] modelled in the forward problem using the `DeTECT` software. From this a Jacobian was calculated for each sensor layout. The singular values of these Jacobians were found using SVD and plotted against each other in comparison. For each Jacobian, the SVD values found were normalised so that the magnitudes could be all compared together with a percentage noise as otherwise they would require individual noise lines on the graph.

Sensor	1	2	3	4	5	Original
Count	44	40	41	49	39	42

TABLE I: Average number of singular values above 1% noise for each sensor design.

If a noise level of 1% is assumed, then a threshold level can be placed at 10^{-2}. Any SVD values that fall below this threshold will be deemed to have such a small affect on the image reconstruction that they will only amplify this 1% of noise. Therefore they will be destructive to the image and removed. For this reason the more SVD values that the Jacobian of a particular sensor has above the threshold, the better the reconstruction of the final image will be.

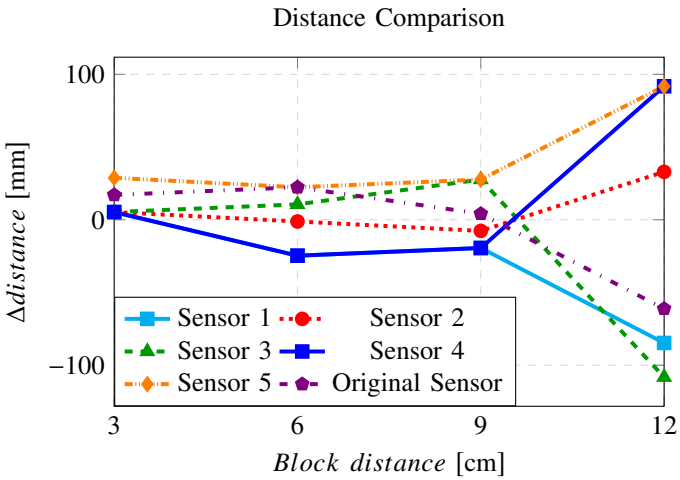

Fig. 9: Difference between detected distance and actual distance of wooden block.

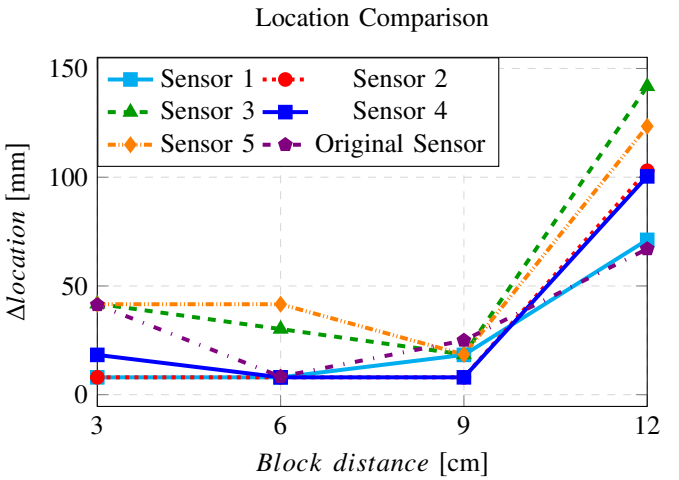

Fig. 10: Difference between detected location and actual location of wooden block.

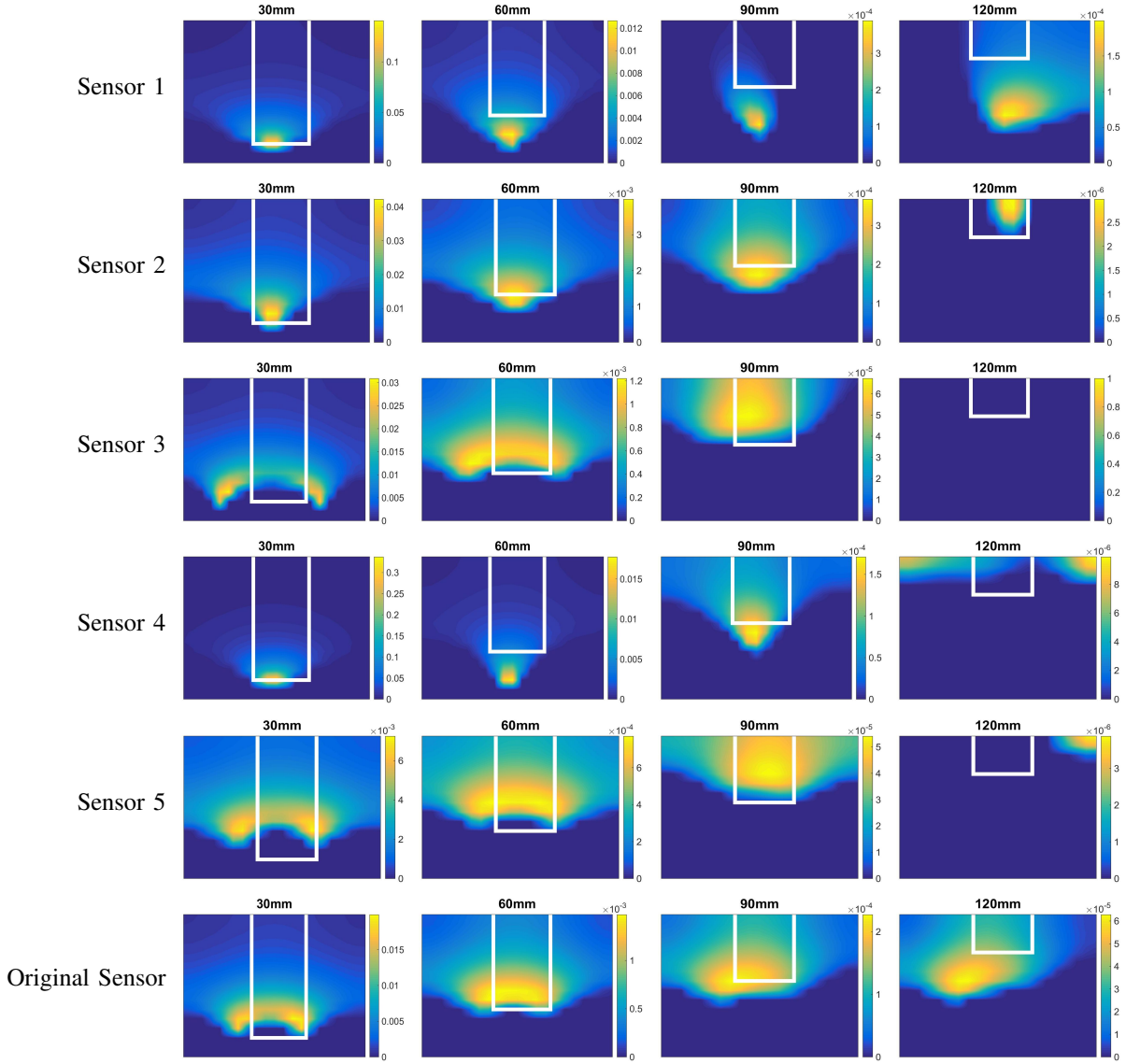

Fig. 11: Reconstruction of permittivity for a wooden block **30mm**, **60mm**, **90mm** and **120mm** from the sensor head.

From figure 8 it can be seen that all of the sensor designs behave very similarly to each other. These results lie within the same range as the simulation results from the procedurally generated designs. The best sensor design, Sensor 4, has 49 out of 66 singular values above the noise threshold and this is only beaten by 4 sensor designs in the simulation results which each achieved 50 singular values above the noise threshold. At lower resolutions the number of singular values is much more erratic which could be due to limitations of the FDM model in `DeTECT` . It seems that stability occurs for resolutions above 20 at which point there is much more consistency showing that the forward problem is operating more accurately. Reconstructions will therefore be performed at or above 20 voxels per dimension.

Depth/Location detection: Detecting the distance and location of an object was performed using a wooden block of dimensions 190mm × 60mm × 45mm. This wooden block is almost identical to the one used in distance reconstruction from Ye et al. (2013) [8]. This will allow for direct comparisons to be made between the results obtained from their experiments and the experiments in this paper. The setup can be seen in figure 5. All of the sensors had background capacitance measurements taken when placed in the exact same place in the test area with no block present. The wooden block was then placed vertically in the viewing area at 30mm, 60mm, 90mm and 120mm referenced from the bottom of the block to the top of the sensor head.

Figure 11 shows the reconstructed images in comparisons to where the actual wooden blocks were located. Visually it would appear that sensors 2, 3, 5 and Original are best at reconstructing the object at the right distances up to 90mm as they are quite accurate at this range. There seems to be no similarity in the features which would explain this. Sensors 1, 2 and 4 reconstruct very small round shapes where sensors 3, 5 and Original reconstruct curved long shapes. Sensors 1, 2 and 4 are made up of a combination of long thin rectangular

electrodes and triangles with many lines of symmetry going through the centre. The other sensors contain far fewer lines of symmetry and do not focus around the centre as much. This might not show that these features are any better or worse for reconstruction but it does show how the shape of the reconstruction can be affected by electrode shape.

All the other sensors reconstruct random shapes at 120mm possibly caused by background interferences due to the weak electric field at such a distance. It could also be due to noise amplified by the singular values located below the noise threshold from SVD analysis.

The maximum point of each reconstructed object was located and the distance, Z, and location, X and Y, of this point was found. This was then compared to the centre of the lowest point on the wooden block and the difference between the actual point on the block and the detected point is plotted on distance and location graphs in figures 9 and 10.

Initially it can be noted that for both location and distance all of the sensors have consistent results up to a block distance of 9cm but after at 12cm the error drastically increases. This supports the results from the reconstructed images in figure 11. For that reason then the following discussions are based on 3cm - 9cm. Looking mainly at the location comparison plot, figure 10, the same distinct groupings of sensors as before can be seen where Sensors 1, 2 and 4 are very similar and the others following a similar trend. When looking at the reconstruction images it was not clear which group reconstructed the image better but here it would appear that Sensors 1, 2 and 4 are better at detecting the location and Sensors 3, 5 and Original are better at detecting the depth (apart from Sensor 2 which is the best at depth too). This gives further indication to the benefits of different electrode shapes and symmetrical designs.

Combined Sensor

One of the limitations of planar array ECT is that the number of measurements, m, is much smaller than to the number of points, n, to calculate. This heavy imbalance causes the problem to be ill-conditioned. If a measurement was taken from each individual sensor of the same object, in the same environment and in the same location then it could be assumed that all of the measurements were from 1 device rather than 5 individual sensors. The reconstruction could then use all of the combined capacitance measurements in order to reconstruct the permittivity distribution.

The combined sensor idea works by essentially switching the shapes of the electrodes in between each set of measurements. In theory the combined sensor has an infinite number of electrode shapes and layouts. Depending on the switching mechanism it could also use a variable number of electrodes rather than a fixed number. This means that each calculation now uses $m \times l$ capacitance measurements, where l is the number of different electrode combinations used. This, in theory, improves the overall solution as more measurements are used to calculate the same number of answers.

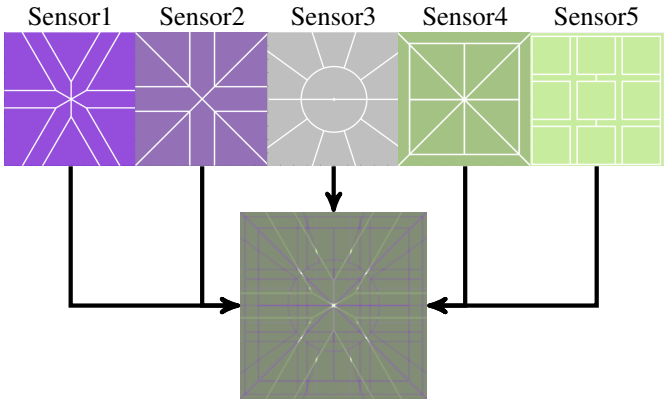

Fig. 12: Visualisation of the combined sensor.

SVD analysis: An immediate benefit can be seen if the same SVD analysis of all the 5 sensor designs combined is compared to the sensors individually. The exact same SVD analysis as earlier was performed on the combined sensor with the same resolution of 30. The results in figure 13 clearly shows the much larger number of singular values available above the noise threshold. The combined sensor had 198 singular values above the noise threshold compared to the best individual sensor which had 49. This means that a lot more information can be obtained as the Jacobian will reconstruct more data not susceptible to noise.

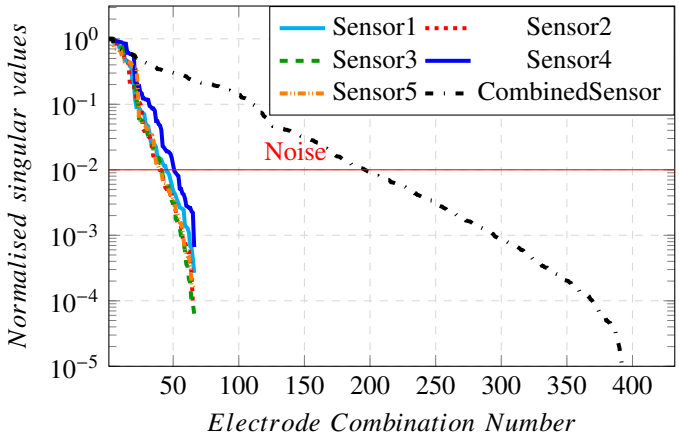

Fig. 13: Combined sensor singular values compared to all the other sensor designs.

To see how the number different sensor designs used in the combined sensor affects the SVD results, the procedurally generated sensor designs were combined into increasingly larger combined sensor combinations. The procedurally generated sensor designs of all 4 design modes were combined in combinations from 2 to 242 sets of sensor designs and then simulated. No design was used in multiple combinations.

Figure 14 shows the singular values increasing in number as the number of individual sensors used in each combination

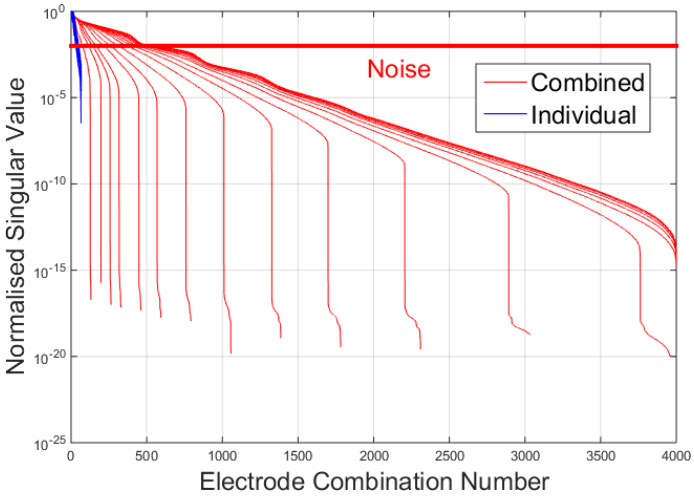

Fig. 14: SVD analysis of increasingly large combinations of procedurally generated sensor designs.

increases. However the number of singular values above the noise threshold does not increase linearly with the number of singular values in total.

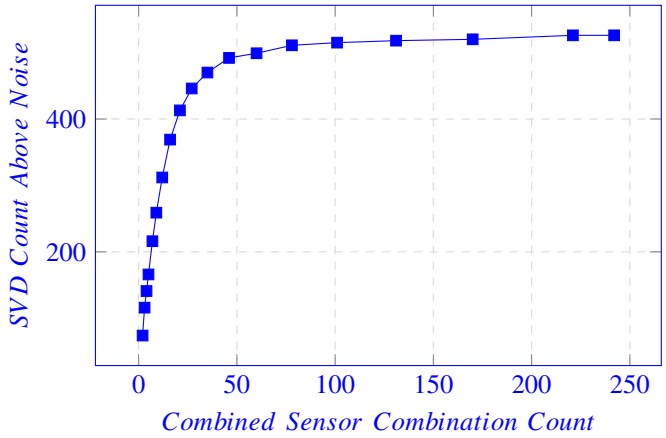

Fig. 15: Comparison of SVD values above noise for increasing number of combinations in combined sensor.

Figure 15 shows the number of singular values above the noise threshold against the number of individual sensor designs used in the combination. It can be seen that for lower sensor counts, adding more sensors to the combined sensor will achieve a big gain in singular values not affected by 1% noise. However this quickly flattens and it would seem that using any more than 100 individual sensors as part of a combined sensor would not produce any useful additional information to the reconstruction.

Depth/Location detection: The increase in data in the Jacobian for the combined sensor should in theory improve the reconstructions. Figure 16 shows the reconstructions of the combined sensor using all 5 of the sensor designs. The reconstructions are accurate in terms of distance/location up to 90mm and even at 120mm an object has been found at the right distance even though it is not in the right location. Looking back at the individual reconstructions in figure 11

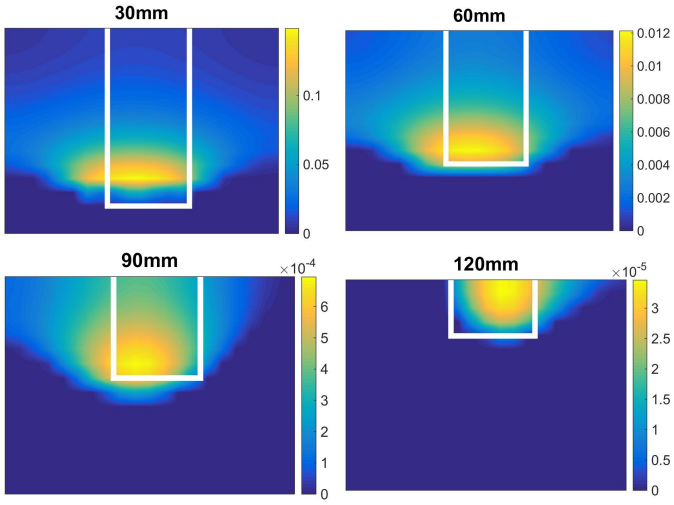

Fig. 16: Combined sensor using all 5 sensor designs reconstructing permittivity at varying distances.

some of the sensors do not perform well at 120mm. This could be due to poor sensor performance or errors in the capacitance readings. Either way these results in theory should actually be degrading the performance of the combined sensor rather than aiding it. However, despite the fact that the combined sensor contains capacitance readings and Jacobians, which on their own cause poor reconstructions at 120mm, it is able to reconstruct the object fairly accurately. This indicates that the combined sensor is able to essentially 'filter' measurements and prevent them from degrading the image too much.

Sandbox Testing

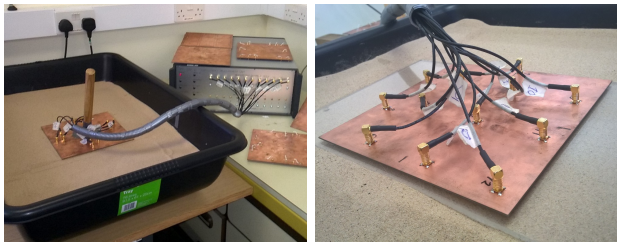

Fig. 17: Sandbox Testing setup.

The permittivity reconstruction tests from figure 11 and 16 are performed in free space, which has a relative permittivity of 1. As dry wood usually has a permittivity somewhere between 2 and 6 the reconstruction is attempting to solve the problem for a positive change in permittivity from the background. In the scenario of a buried landmine however, it could be surrounded by a higher permittivity environment and therefore the reconstruction of this will be significantly harder as a weaker signal surrounded by strong signals is trying to be reconstructed. A landmine could have areas of both lower and higher permittivity than the surrounding ground. To test the performance of the sensors in more a of a 'landmine' type scenario a sandbox was used. The relative permittivity of dry

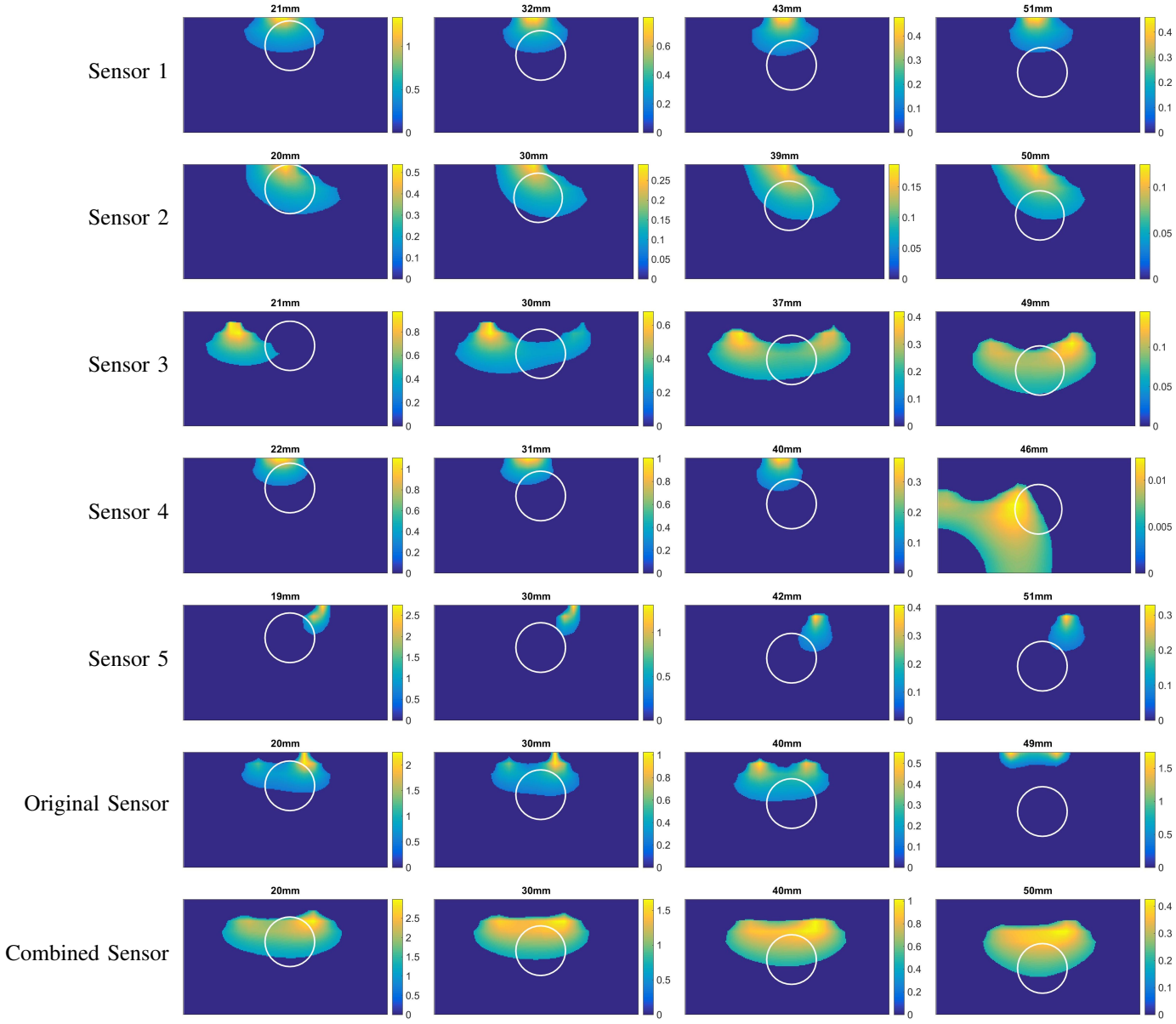

Fig. 18: Sandbox testing reconstructions of water bottle at various depths.

sand lies in the region of 2.5 to 3.5. A mostly filled bottle of water was used to simulate a foreign object in the sand where the water and air have a relative permittivity close to 90 and 1 respectively. The water bottle had a diameter of 56mm, height of 120mm and was 80% full of tap water.

The water bottle was buried in dry sand from distances ranging between 20mm - 90mm from the sensor head. The sensors where then placed on top of the sand with a thin perspex sheet shielding the electrodes from direct contact with the sand as shown in figure 17. Due to a high sensitivity area near the sensor head, the reconstructions were created by removing 2 planes of pixels so that the reconstruction started approximately 10mm away from the sensor head. Also as each sensor is slightly different in construction, accurate measurements of sensor head to sand surface distance were taken and included in the reconstructions. This means that the stated depth above each image of the sandbox reconstructions in figure 18 is the distance from the water bottle to the sensor electrodes but the image is only showing the reconstructed area below the surface of the sand. As the aim of sandbox was to evaluate the ability of the sensors to detect sub surface objects, they are not evaluated based on the optimisation criteria. Due to there being a slight gap between the sensor electrodes and the surface of the sand, caused by the perspex and slight air gap, there is a lot of both positive and negative reconstruction noise near the surface. Therefore the reconstructions were segmented using Otsu thresholding [15] to only capture the inclusion.

As before with the individual reconstructions the 2 distinct groups of sensors is appearing. Sensors 1, 2 and 4 reconstruct a object with the right shape but the depth is not accurate. The other sensors are much better at getting a more accurate depth

but the object shape is very poorly reconstructed. Sensors 1, 2 and 4 have a large concentration of electrodes in the middle which could be resulting in a very highly sensitive region there. This could mean that they are able to reconstruct location and shape very well but only when the object is only directly located above this area. Sensors 3, 5 and Original however have their electrodes spread out much more and this could be creating more of a dome shape in the Jacobian which leads to much better depth detection but will produce this curved dome shape reconstruction.

The combined sensor reconstructs a very consistent shape and also although the actual depth in the reconstructions is not very accurate it is still showing an increase in the depth of the segmented inclusion as the actual depth increases. This shows that it is being affected by the increasing depth. Furthermore when looking at the colours of the segmented inclusions for all sensors it becomes apparent that the combined sensor is producing a much stronger inclusion reconstruction. The colours in the inclusion represent higher values and most of the sensors reconstruct an inclusion made up of a core of yellow, representing a high permittivity, and surrounded by a large area of blue, representing an area of lower permittivity. The combined sensor however has a very large core of yellow and then a much smaller surrounding area of green which indicates that the inclusion has a much larger difference in permittivity to the background than the individual sensors could reproduce. The permittivity gradient between the water bottle and the surrounding sand is very distinct and so the reconstructions should shows this. Instead most of them show a gradual permittivity shift from the water to the sand but the combined sensor has the greatest gradient shift between highest permittivity and the edge indicating that it is producing the most accurate representation of the object.

The individual sensors can be grouped into 2 distinct groups based on their reconstruction performance in both air and sand with the wooden block and water bottle. These the 1st group is able to reconstruct locations and shapes better but the 2nd group is able to reconstruct depth much more accurately. It then makes sense that a combinations of these sensor design features would be best to get the best single reconstruction. This is exactly what the combined sensor appears to do and it produces reconstructions which show benefits from both groups of sensor designs.

VII. Conclusion

Initially over 7000 sensor designs were procedurally generated in a random manner to create a large variation of unique designs which had 4 different modes of constraints. These were then simulated with `DeTECT` and their ability to theoretically reconstruct an image was recorded. From these results it was found that symmetry in the sensor design had a very large bearing on performance, with more lines of symmetry showing a better ability to reconstruct an image. The simulation hinted at features, such as symmetrical electrodes, thin electrodes and curved electrodes, which were beneficial to ECT sensor design which could then be considered when designing new sensors.

Five new sensor designs were created to be tested experimentally. Using the newly developed `DeTECT` software, the designs were tested both theoretically, with SVD analysis, and practically, by imaging a wooden block suspended above them.

SVD analysis of the individual sensor designs showed that Sensor 4 theoretically had the best design to reconstruct the most noise free data from capacitance data. A look at the sensitivity plots showed that Sensor 4 had a unique sensitivity shape compared to the others which were all very similar. This shape could be due to the outer electrodes encasing the inner electrodes and maybe directing the sensitivity region leading to potential increases in performance indicated by the SVD analysis.

The reconstructions of the wooden block showed that all the designs could locate the block with reasonable accuracy between 30-90mm but none of them produced good results at 120mm although sensor 4 and 5 could at least reconstruct some resemblance of the block but at the wrong depth. This is in line with other planar array ECT work which indicates a depth detection limitation at approximately the same distance as the furthest electrode pairing which in this case was approximately 100mm on average.

When looking at the features specifically it was noticed that results in distance and location detection grouped the sensors into 2 groups. Analysis of these groups found that group 1, sensors 1, 2 and 4, had very similar features, as did group 2, sensors 3, 5 and Original. Group 1 had long thin rectangular electrodes and triangular electrodes meeting at the middle producing a lot of lines of symmetry. Group 2 did not focus on the centre as much and had a greater average distance between electrodes. Electrodes focused around the centre appeared to produce better location detection and shape reconstruction but this could also just be down to the fact that the object were placed in the centre were they are most sensitive. Increasing the average distance between electrodes improved the depth detection capability of the reconstruction but degraded the reconstruction of the object shape.

It was theorised that by combining all of the sensor measurements together, along with the Jacobians, much more accurate reconstructions could be achieved. This theory was aided by the SVD analysis of a combination of all the sensors which showed that the combined sensor had over 3 times more useful measurements than the best individual sensor. This was supported by combining increasing numbers of the procedurally generated sensor designs and running the same SVD analysis on these combinations. The simulation results showed that after combining up to 100 unique sensors in the combined sensor, the amount of additional information gained by adding more was not very significant. But at low numbers (less than 100 combined sensors) a lot of additional noise free information could be retrieved by using more sensors.

Experimental reconstructions using the 5 individual sensor designs combined showed an improvement in object location

and distance reconstruction when compared with each sensor design individually. It also showed that increasing the number of sensors used in reconstruction would be beneficial even if some of the sensors were poor as the overall combined sensor could in some way 'filter' out the effect of these poor sensor designs. Therefore there is reason to believe that the more sensors used in combination the more accurate the reconstruction will be up to a point.

When the sensors were tested in a setting more common with landmine detection, buried in sand, the combined sensor again showed that it was able to reconstruct the image with greater consistency and also with a better defined shape.

The reconstructions of objects in both sand and air could possibly be improved by changing the reconstruction algorithm. As there is a clear permittivity difference between object and background the final reconstruction shouldn't be producing a gradual permittivity change, but instead a very quick one showing a clear boundary between regions. The Tikhonov algorithm is poor at this and improved reconstructions could be achieved by instead using a Total Variation based algorithm which looks at removing increasing gradients in reconstruction and finding regions of constant permittivity. The Tikhonov algorithm also has inherent problems with depth detection when the object is far away and so depth could possibly also be improved by changing the reconstruction method.

These results bode well for using planar array ECT for landmine detection because they show that it is possible that by simply changing the shape and layout of the electrodes on the sensor head, an improvement in depth detection and shape reconstruction can be achieved. This is useful as it is a very quick and cheap method of improvement. If a combined sensor could be made that could switch to be any sensor design, then this would theoretically be able to produce even better results as well as continue to find the optimal design by physically testing many more features in a more rigorous manner.

Acknowledgement: This work is sponsored by Find A Better Way, a landmine detection and clearance charity and the University of Bath Alumni Fund.

REFERENCES

[1] M. K. Habib. (2002) Mine clearance techniques and technologies for effective humanitarian demining. [Online]. Available: http://www.jmu.edu/cisr/journal/6.1/features/habib/habib.htm

[2] S. M. Huang, A. B. Plaskowski, C. G. Xie, and M. S. Beck, "Capacitance-based tomographic flow imaging system," *Electronics Letters*, vol. 24, no. 7, pp. 418–419, March 1988.

[3] W. Yang, "Design of electrical capacitance tomography sensors," *Measurement Science and Technology*, vol. 21, no. 4, 2010.

[4] A. V. Mamishev, K. Sundara-Rajan, F. Yang, Y. Du, and M. Zahn, "Interdigital sensors and transducers," *Proceedings of the IEEE*, vol. 92, no. 5, pp. 808–845, May 2004.

[5] A. Somerville, I. Evans, and T. York, "Preliminary studies of planar capacitance tomography," in *Proceedings of the 1st World Congress on Industrial Process Tomography, Buxton, Greater Manchester*, vol. 1417, 1999, p. 522529.

[6] R. Keeley, "Understanding landmines and mine action," September 2003.

[7] X. Hu and W. Yang, "Planar capacitive sensors âĂŞ designs and applications," *Sensor Review*, vol. 30, no. 1, pp. 24–39, 2010.

[8] Z. Ye, R. Banasiak, and M. Soleimani, "Planar array 3d electrical capacitive tomography," *Insight*, vol. 55, no. 12, pp. 675–680, December 2013.

[9] R. Penrose, "A generalized inverse for matrices," *Mathematical Proceedings of the Cambridge Philosophical Society*, vol. 51, pp. 406–413, 7 1955.

[10] A. Neubauer, "Tikhonov regularisation for non-linear ill-posed problems: optimal convergence rates and finite-dimensional approximation," *Inverse Problems*, vol. 5, no. 4, p. 541, 1989.

[11] M. Hanke, A. Neubauer, and O. Scherzer, "A convergence analysis of the landweber iteration fornonlinear ill-posed problems," *Numerische Mathematik*, vol. 72, no. 1, pp. 21–37, 1995.

[12] M. Enokizono, E. Kato, and Y. Tsuchida, "Inverse analysis by boundary element method with singular value decomposition," *IEEE Transactions on Magnetics*, vol. 32, no. 3, pp. 1322–1325, May 1996.

[13] M. Soleimani, "Numerical modelling and analysis of the forward and inverse problems in electrical capacitance tomography," *International Journal for Information & Systems Sciences*, vol. 1, no. 2, pp. 193–207, 2005.

[14] M. Soleimani and W. R. B. Lionheart, "Nonlinear image reconstruction for electrical capacitance tomography using experimental data," *Measurement Science and Technology*, vol. 16, no. 10, p. 1987, 2005.

[15] N. Otsu, "A threshold selection method from gray-level histograms," *IEEE Transactions on Systems, Man, and Cybernetics*, vol. 9, no. 1, pp. 62–66, Jan 1979.